The submitted manuscript has been authored by a contractor of the U. S. Government under contract No. W-31-109-ENG-38. Accordingly, the U. S. Government retains a nonexclusive, royalty-free license to publish or reproduce the published form of this contribution, or allow others to do so, for U. S. Government purposes.

ANL-HEP-CP-93-99

ANL-HEP-CP-93-99

Fermilab Library
0 1160 0024254 2

DEC 20 1993

DEEP INELASTIC SCATTERING RESULTS FROM THE FIRST YEAR OF HERA OPERATION

STEPHEN R. MAGILL
HEP Division, Argonne National Laboratory
Argonne, Illinois 60439, USA

ABSTRACT

The first year of operation of the HERA electron - proton collider has resulted in Deep Inelastic Scattering (DIS) Physics results from both the H1 and ZEUS experiments. Reported here are the H1 and ZEUS measurements of the proton structure function F_2 at higher Q^2 and lower x than previously reported from fixed target experiments. Also included are the results of QCD studies on hadronic final states and jets, and the observation of high Q^2 charged current events from both experiments. Finally, the observation of events with large rapidity gaps by the ZEUS collaboration is also reported.

1. Introduction to HERA

The HERA electron-proton collider at DESY[1] began operation in 1992, delivering $\sim 30\ nb^{-1}$ of luminosity to the H1 and ZEUS detectors. Presented here are results of the analyses of Deep Inelastic Scattering (DIS) events from both H1 and ZEUS from this first year's run. The results include the measurement of the structure function F_2 at significantly lower x than has been seen so far, measurements of energy distributions and jet production in the hadronic final state with comparisons to various Monte Carlo models, the observation of charged current DIS events, and the first observation of events with large rapidity gaps by the ZEUS Collaboration.

In this first running period, the instantaneous luminosity obtained by HERA was $\sim$ 1/300 of the design goal stated for the accelerator. Much of this factor is expected to be made up in the current year's run (1993). These first results are indicative of the wide range of interesting topics in DIS physics which will be explored in even more detail in the future.

2. Detectors at HERA

The H1 and ZEUS detectors are both large, multi-purpose detectors which rely on accurate charged particle tracking in a magnetic field, precise electromagnetic and hadronic calorimetry, and muon detection, in order to study aspects of

high Q^2 processes (DIS neutral current and charged current events), low Q^2 processes (photoproduction and diffractive physics), and searches for exotic processes (leptoquarks and leptogluons, and excited electrons).

2.1. The H1 Detector

Figure 1 shows a cutaway view of the H1 detector which is described in detail elsewhere[2]. In this paper, only those components of the detector used for the analyses reported here will be discussed.

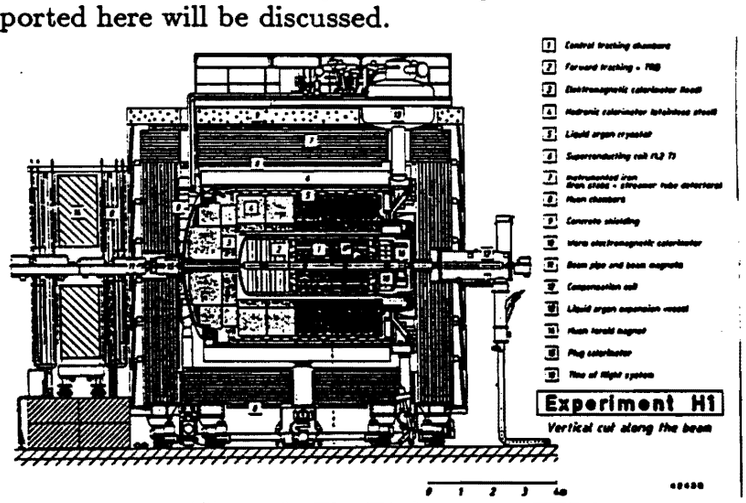

Figure 1: The H1 detector at HERA.

Charged particles originating at the interaction point are tracked in the forward, central, and backward tracking chambers. The forward tracker is made of 3 modules of drift chambers and multiwire proportional chambers. It provides coverage in polar angle, θ, from 7° to 25°. The central tracker consists of two jet drift chamber modules, two longitudinal drift chambers, and two multiwire proportional chambers for triggering. The polar angle coverage of these chambers is $15° < \theta < 170°$. The backward tracker is made of 4 wire planes of multiwire proportional chambers and has an angular acceptance of 155° to 175°.

Calorimetry is provided by a liquid argon calorimeter covering the forward and central regions and the Backward Electromagnetic Calorimeter (BEMC). The BEMC is made of lead-scintillator sandwich stacks corresponding to a depth of 22 X_0 and provides coverage in θ from 154° to 176°. The energy resolution of the BEMC is $\sigma(E)/E = 0.11/\sqrt{E}$ for electrons. The liquid argon calorimeter has an electromagnetic section with lead absorber and a hadronic section with steel absorber, covering polar angles from $4° < \theta < 155°$. The total depth of the liquid argon calorimeter varies from 4.5 to 8 interaction lengths. The energy resolutions for the liquid argon calorimeter are $\sigma(E)/E = 0.12/\sqrt{E}$ for electrons and $\sigma(E)/E = 0.50/\sqrt{E}$ for hadrons.

The liquid argon calorimeter and the tracking detectors are surrounded in the central region by a superconducting solenoid which provides a uniform field of 1.2 *Tesla*.

A Time-of-Flight (TOF) system, located behind the BEMC and consisting

of two scintillator planes with a time resolution of 3 ns, allows the vetoing of proton beam-gas events occuring upstream of the detector.

The e-p luminosity was measured by tagging electrons and photons in coincidence and comparing to the known rate of the bremstrahlung process $ep \to ep\gamma$. Both the electron detector and the photon detector are $TlCl/TlBr$ crystal calorimeters.

2.2. The ZEUS Detector

Figure 2 shows a cutaway view of the ZEUS detector. The details of the components of the ZEUS detector are described elsewhere[3]. Again, only the components used in the analyses reported in this paper will be discussed here.

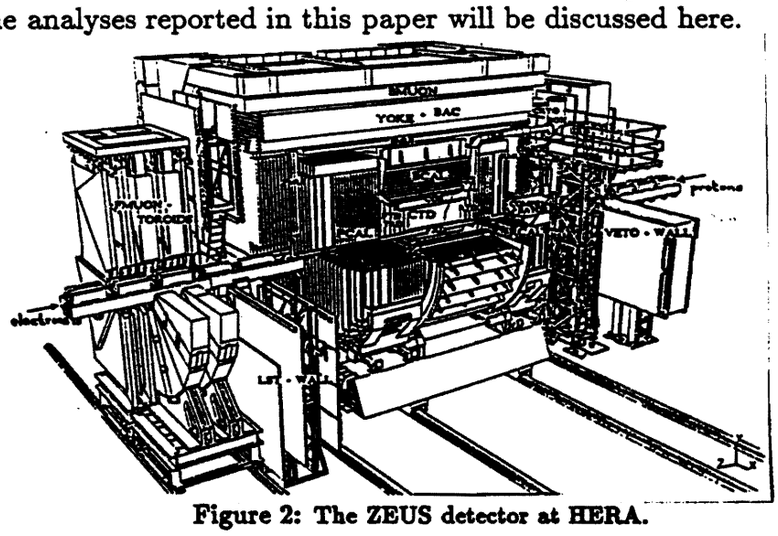

Figure 2: The ZEUS detector at HERA.

The principle component used in the ZEUS DIS analyses is the uranium scintillator calorimeter[4] with photomultiplier tube (PMT) readout. The three sections, forward (FCAL), barrel (BCAL), and rear (RCAL), were constructed in an identical manner using alternating layers of uranium sheets and scintillator tiles. The relative thickness of the components of this sandwich structure was chosen to make the calorimeter fully compensating. The depth of the calorimeter is 7 interaction lengths in the FCAL, 5 in the BCAL and 4 in the RCAL, measured at normal incidence. The calorimeter provides coverage in polar angle, θ, ranging from 2.2° to 176.5°, which represents 99.7% of 4π. The resolution of the calorimeter has been measured in test beams[4,5] to be $\sigma(E)/E = 0.18/\sqrt{E}$ for electrons and $\sigma(E)/E = 0.35/\sqrt{E}$ for hadrons where E is in GeV. The calorimeter yields a time resolution of < 1 ns for energy deposits > 4.5 GeV. The calibration of the calorimeter is stable to $\sim 0.2\%$ and was monitored using the uranium noise signal, charge injection to the input of the readout electronics, and light from LEDs and lasers incident at the face of the PMTs.

Charged particle tracks are measured in the central tracking detector (CTD)[6] which surrounds the beampipe. This chamber consists of 72 drift chamber layers arranged in 9 superlayers. In 1992, three superlayers were instrumented with Z-

by-timing readout electronics. The CTD tracks provided a vertex resolution of $\sigma_Z = 4\ cm$ and $\sigma_{XY} = 1\ mm$.

A thin (0.9 radiation length) superconducting solenoid is located inside the calorimeter, surrounding the tracking chambers. The solenoid was operated with a central magnetic field of 1.43 *Tesla*.

Two lead scintillator counters (C5) partially surround the beampipe at the rear of the RCAL. These were used as a veto in the trigger for proton - gas background and to measure the timing and longitudinal spread of both the electron and proton beams. An instrumented iron vetowall, upstream of the detector, was also used to veto beam halo background.

The e-p luminosity was measured by tagging electrons and photons in coincidence in the same manner as in the H1 detector. Both the electron detector and the photon detector are lead-scintillator sandwich calorimeters.

3. Deep Inelastic Scattering Kinematics at HERA

The DIS process is mediated by the exchange of a virtual boson, usually a virtual photon at low x and low Q^2, between the incoming electron and proton. If the momentum transfer (q) is large enough, the proton breaks up into a struck quark and the proton remnant which fragment into the observed final state particles. The important kinematic variables in DIS are the square of the four momentum transfer, Q^2, the fraction of the momentum carried by the struck quark, $x \equiv x_{Bj}$ in the frame in which the incoming proton momentum is large, and the normalized fraction of energy transferred, y. These variables can be determined several ways using information gathered by the detectors from the scattered electron and final state hadrons[7]. From the scattered electron energy (E'_e) and polar angle (θ'_e) :

$$Q^2 = 2E_eE'_e(1 + \cos\theta'_e) \tag{1}$$

$$y = 1 - (E'_e/E_e)(1 - \cos\theta'_e)/2 \tag{2}$$

where E_e is the electron beam energy. The Jacquet-Blondel method gives :

$$Q^2 = \sum_h (p_x^2 + p_y^2)/(2E_e) \tag{3}$$

$$y = \sum_h (E - p_z)/(2E_e) \tag{4}$$

where the sums are performed over all of the hadrons. In addition to these, the "Double Angle Method" can be used which determines the kinematic variables from the polar angles of the scattered electron and the hadronic system. The angle of the hadronic system (which is the scattered angle of the struck quark in the Quark Parton Model (QPM)), is given by :

$$\cos\gamma_h = \frac{(\sum_h p_x)^2 + (\sum_h p_y)^2 - (\sum_h (E - p_z))^2}{(\sum_h p_x)^2 + (\sum_h p_y)^2 + (\sum_h (E - p_z))^2} \tag{5}$$

and the kinematics are given by :

$$Q^2 = \frac{4E_e'^2 \sin\gamma_h(1+\cos\theta_e')}{(\sin\gamma_h + \sin\theta_e' - \sin(\gamma_h+\theta_e'))} \tag{6}$$

$$y = \frac{\sin\theta_e'(1-\cos\gamma_h)}{(\sin\gamma_h + \sin\theta_e' - \sin(\gamma_h+\theta_e'))} \tag{7}$$

The variable x, is determined from the relation $x = Q^2/sy$, where s is given by $s = 4E_eE_p$, and E_p is the proton beam energy. Figure 3 shows the $x - Q^2$ kinematic plane at HERA with contours of scattered electron energy and angle and also current jet energy and angle. The current jet energy and angle are calculated from the kinematic variables and correspond to the properties of the struck quark in the QPM.

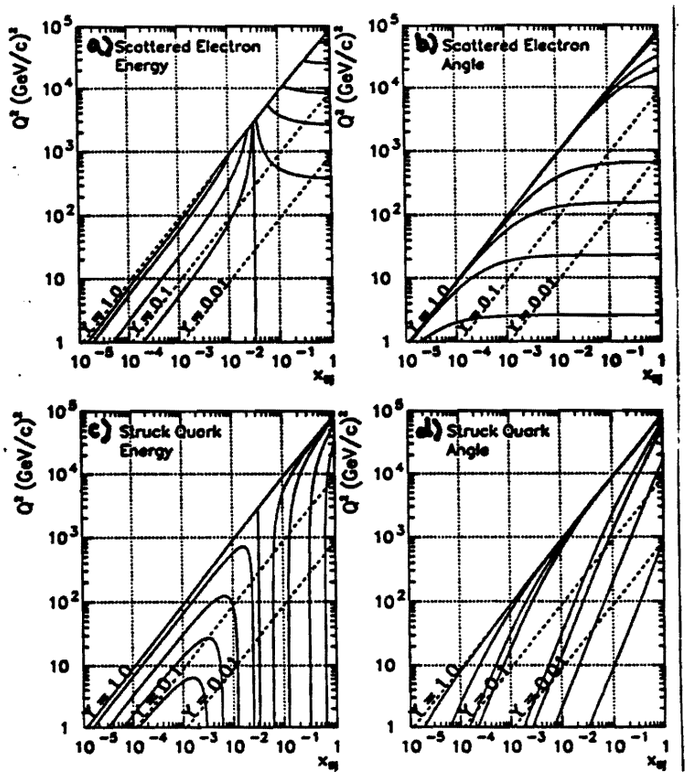

Figure 3: $x - Q^2$ kinematic plane at HERA with contours of (a) scattered electron energy which is dominated by the kinematically favored $E_e' = 26.7\ GeV$ at $x = 26.7/820 = 0.033$, (b) scattered electron angle with the smallest angle corresponding to the edge of the ZEUS RCAL at low Q^2, (c) QPM current jet energy again showing the singularity at $E = 26.7\ GeV$, and (d) QPM current jet angle with the angle corresponding to the forward edge of the ZEUS FCAL shown at very low y.

4. Deep Inelastic Scattering Results

4.1. Proton Structure Function F_2

Fixed target experiments have measured the proton structure function F_2 very precisely[8] down to $x = 0.008$, at $Q^2 < 4\ GeV^2$. At HERA, F_2 can also be measured, but at higher Q^2 values and at very low x, e.g., $Q^2 = 10\ GeV^2$ at $x = 1\times10^{-4}$. For the first time, the transition between perturbative and non-perturbative QCD can be studied in the low x region.

The structure function F_2 is related to the measured neutral current DIS cross section according to the formula :

$$\frac{d^2\sigma}{dxdQ^2} = \frac{2\pi\alpha_{em}{}^2}{xQ^4}[2(1-y) + \frac{y^2}{(1+R)}]F_2(x,Q^2) \tag{8}$$

where R is the ratio of longitudinal to transverse cross sections for virtual photon absorption. In both the H1 and ZEUS analyses, a suitable value for R is chosen and the variation of the resultant F_2 measurement with R becomes part of the reported systematic error. In the limit of large proton momentum, F_2 is related to the parton distributions by :

$$F_2 = x\sum(q_i + \overline{q_i}) \tag{9}$$

and so is a measure of the number of quarks and anti-quarks (weighted by their momentum fraction) in the proton.

The H1 analysis was done in two independent ways as a check on the size of the systematic errors. The first method used only the scattered electron variables to determine the event kinematics. The bins were chosen corresponding to detector variables $\sqrt{E'_e}$ and θ'_e. The radiative tail was subtracted in one pass. This method minimized the unknown structure function dependence for the corrections, which was included in the estimate of the systematic error. The second analysis was done in bins of x and Q^2, where these variables were calculated using a "mixed" method involving both the electron and hadronic variables. Radiative corrections were applied multiplicatively and the procedure was iterated several times until the result was constant within errors. A special bin was evaluated at $Q^2 = 15\ GeV^2$ and for the x range from $0.01 - 1$. This point was used as a normalization check by comparing it with the fixed target NMC and BCDMS results[8]. Figure 4 shows the F_2 results from the H1 collaboration for the two methods used and the normalization point. The measured F_2 values are compared to the NMC and BCDMS results and several F_2 parametrizations generated from fitted parton distribution functions[9]. A 12% normalization uncertainty applies to all points and is not included in the systematic errors.

The ZEUS analysis was done in bins of x and Q^2, using the double-angle method to calculate the kinematic variables. Multiplicative radiative corrections were applied iteratively until the resultant F_2 value converged within errors. The

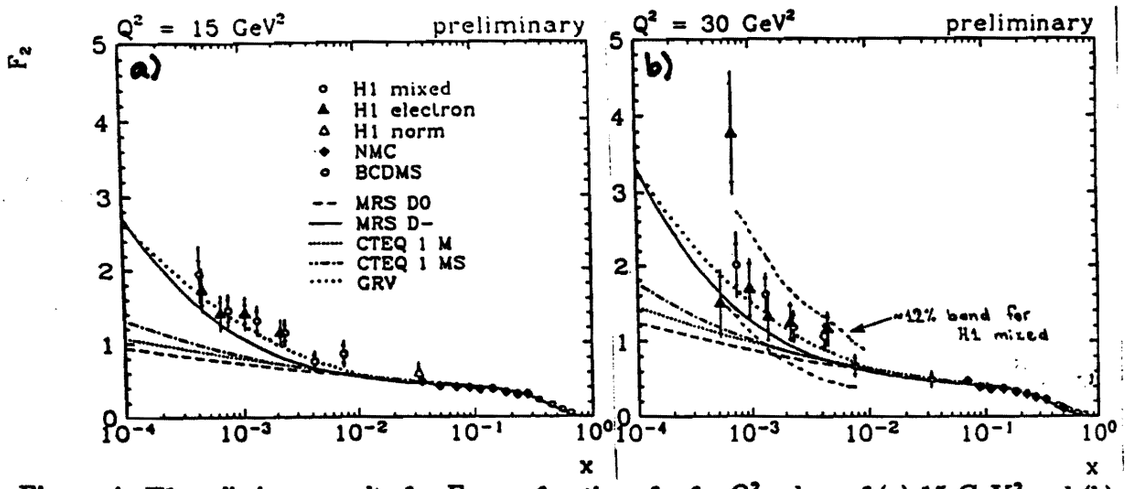

Figure 4: H1 preliminary results for F_2 as a function of x for Q^2 values of (a) 15 GeV^2 and (b) 30 GeV^2.

estimate of the final systematic errors was done by repeating the analysis in several different ways; applying different event selection cuts, using only the scattered electron variables, changing the input structure function, and changing the calorimeter energy scale. In all bins, the largest deviation was never more than one standard deviation away from the nominal result as calculated from the statistics of the bin. Figure 5 shows the F_2 results from the ZEUS collaboration compared to several F_2 parametrizations[9] as a function of x for various Q^2 values, and as a function of Q^2 for various x values with the NMC results overlaid[8]. In addition to the statistical

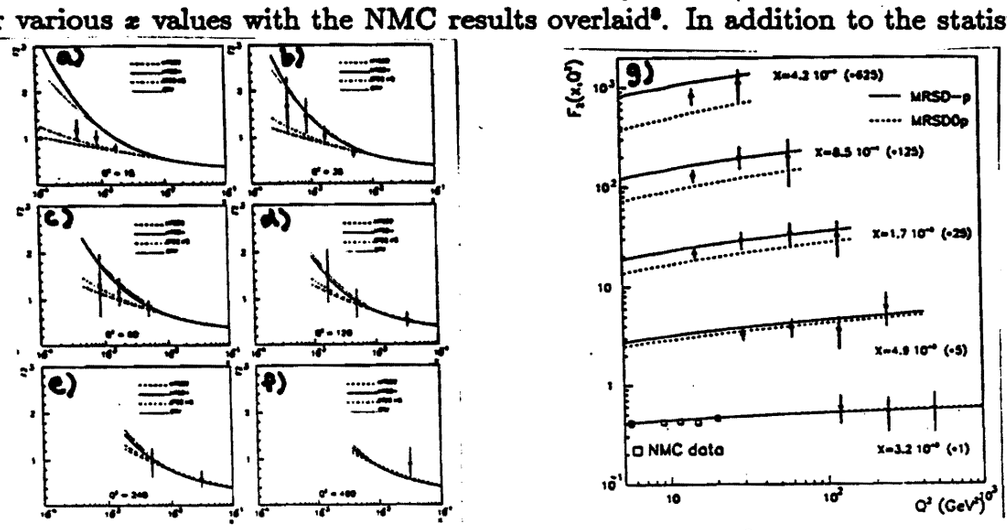

Figure 5: ZEUS preliminary results for F_2 as a function of x for Q^2 values of (a) 15 GeV^2, (b) 30 GeV^2, (c) 60 GeV^2, (d) 120 GeV^2, (e) 240 GeV^2, (f) 480 GeV^2, and (g) as a function of Q^2 for the various x values as indicated including the multiplicative factors in parentheses used for display purposes.

and systematic error bars as shown, a 5% normalization uncertainty applies to all

points.

In Figure 6, the results from H1 and ZEUS are compared for the two common bins of $Q^2 = 15\ GeV^2$ and $Q^2 = 30\ GeV^2$. The results are consistent within

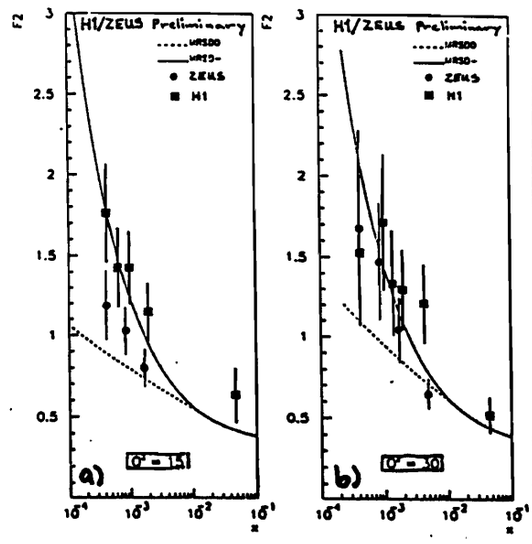

Figure 6: Comparison of the F_2 results from H1 and ZEUS as a function of x in the bins (a) $Q^2 = 15\ GeV^2$ and (b) $Q^2 = 30\ GeV^2$.

the measured statistical errors, estimated systematic errors, and the normalization uncertainties. Both indicate a steep rise in F_2 at low x.

4.2. Hadronic Final States and Jets

The final state hadron energy flow was evaluated by both experiments in several ways with particular emphasis on comparison of the results to various QCD-based Monte Carlo models. Jet production has also been investigated, leading to preliminary measurements of the $(2+1)$ jet rate as a function of Q^2, a measure which is very sensitive to the value of the basic QCD quantities Λ and α_s (and also the gluon content of the proton). At present, the Monte Carlo models used in DIS include subprocesses to $\mathcal{O}(\alpha_s)$ exactly, employing various approximations to simulate the higher order contributions. The measurements described here are sensitive to the value of the higher order contributions, and therefore can be used to check different approximation schemes and to push the theoretical calculation of exact higher order terms.

The first measurements from HERA were compared to 3 different parton level treatments of the DIS process coupled with two different final state fragmentation schemes. The basic method used to describe the DIS process has been the Lund matrix element (ME) calulation to $\mathcal{O}(\alpha_s)$ with hadronization determined by a string fragmentation model[10]. Since higher order QCD processes are needed to describe the data, several attempts to include them have been tried - namely Lund parton showers (PS)[11] and the ARIADNE Color Dipole Model (CDM)[12]. The Lund parton

shower Monte Carlo with string fragmentation was compared to the data with the struck quark maximum virtuality scale set by the different choices - Q^2 (PS(Q^2)), W^2 (PS(W^2)), and $Q^2(1-x)max(1, \ln(1/x))$ (PS($Q^2(1-x)$)). Also, the Lund matrix element calculation to $\mathcal{O}(\alpha_s)$ was used to determine the initial hard scattering, with higher order processes simulated by the addition of parton showers with the scale set by the $\mathcal{O}(\alpha_s)$ hard process (ME+PS). This model also uses string fragmentation to hadronize colored objects. In addition, the HERWIG parton shower scheme with a cluster fragmentation model[13] was compared to the data both with and without the addition of a soft underlying event (SUE). Finally, the Color Dipole Model with string fragmentation was used with the inclusion of the boson - gluon fusion subprocess (CDM+BGF).

The first result shown in Figure 7a is the average transverse momentum squared as a function of $x_{Feynman}$ for positive $x_{Feynman}$ in the hadronic center-of-mass frame as reported by H1[14]. This is one half of the well-known "seagull plot". In the ZEUS detector, "condensates" are formed using a clustering algorithm which

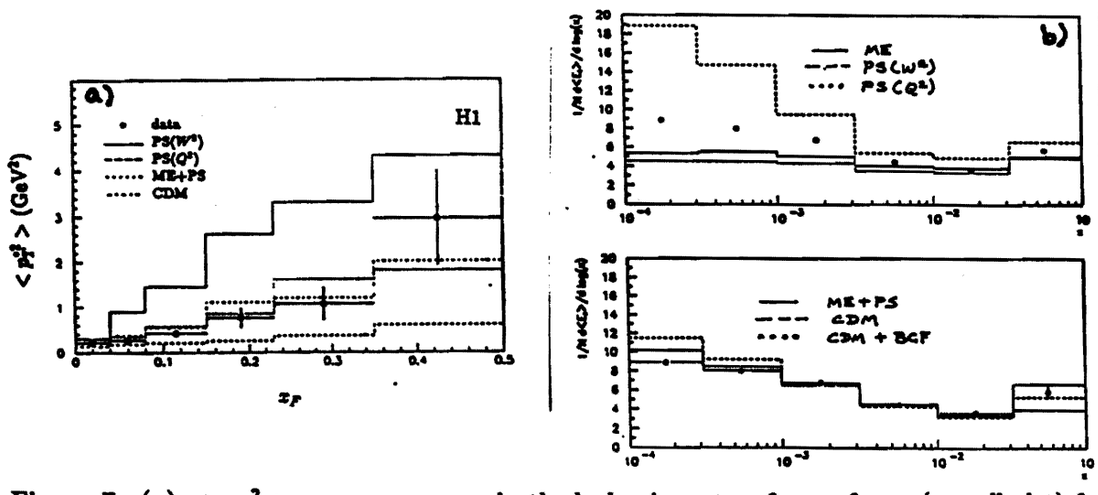

Figure 7: (a) $< p_T{}^2 >$ versus $x_{Feynman}$ in the hadronic center-of-mass frame (seagull plot) for $x_{Feynman} > 0$ compared to several Monte Carlo models from H1, and (b) E_T weighted x distribution of events compared to several Monte Carlo models from ZEUS.

combines adjacent calorimeter cells with energy deposits. Monte Carlo studies using this algorithm show that the correlation between condensates and final state particles is very good in the region used in this analysis. Figure 7b shows the transverse energy (E_T) weighted calorimeter condensate distribution as a function of x compared to the various Monte Carlo models mentioned.

The final state hadron energy flow was also evaluated in terms of γ_h, the polar angle of the hadronic system[15], and $\Delta\eta$, which is defined as $\eta_{calorimeter\ cell} - \eta_{QPM\ Jet}$ where $\eta_{QPM\ Jet}$ is calculated from the quantity γ_h as $\eta_{QPM\ Jet} = -0.5 \ln(\tan(\gamma_h/2))$. For $x < 10^{-3}$, γ_h points in the backward direction. Figure 8 shows the energy weighted $\Delta\eta$ distribution at low x ($x < 10^{-3}$) from the ZEUS collaboration, again compared to the models described above.

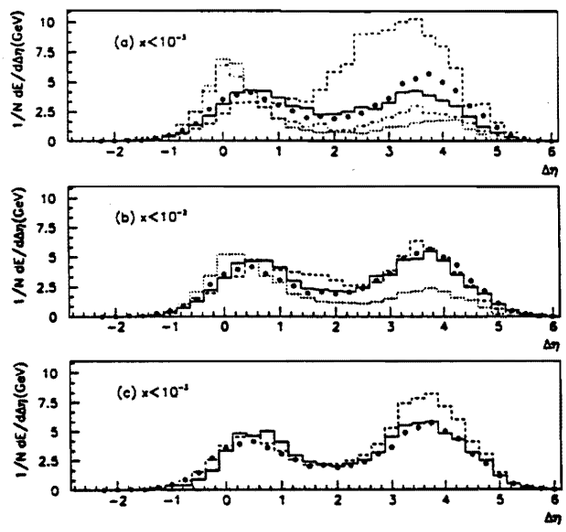

Figure 8: The energy weighted $\Delta\eta$ of the hadronic system with respect to γ_h at low x. The ZEUS data points are shown as dots. In (a), the full histogram is ME+PS, dashed is PS(W^2), dotted is PS(Q^2), and dash-dotted is ME. In (b), the full histogram is CDM+BGF, dashed is CDM, and dotted is PS($Q^2(1-x)$). In (c), the full histogram is HERWIG without the SUE and the dashed histogram is HERWIG including the SUE.

The data reveal several interesting features of the hadron energy flow. As x decreases, the transverse energy of the hadronic system increases. In the $\Delta\eta$ analysis at low x ($x < 10^{-3}$), the current peak in the data is shifted towards the remnant (large $\Delta\eta$) with most of the energy appearing between the expected value of γ_h and the remnant. For both the H1 seagull plot and the ZEUS energy distributions, the predictions of the Color Dipole Model with boson-gluon fusion (CDM+BGF), the Lund ME+PS, and the HERWIG parton shower model reasonably describe the data. In contrast, the Lund ME and the Lund PS models, scaled by the three choices indicated above, fail to describe the data.

The multi-jet analyses of both H1 and ZEUS were done using calorimeter cells as input to the jet-finding algorithm. The algorithm used is the JADE algorithm[16] with a pseudoparticle carrying the missing longitudinal momentum in the event into the forward beampipe. Calorimeter cells are merged into jets by comparing the invariant mass of two cells to a pre-determined cutoff parameter, y_{cut}, which defines the jet resolution. The jet counting notation used always counts the proton remnant jet (corresponding to the jet formed by the pseudoparticle) as +1, with the other jets in the event each counted separately. In this way, $(0+1)$ means that the current jet and remnant jet are merged, $(1+1)$ corresponds to the basic QPM process, and $(2+1)$ jets represent the $\mathcal{O}(\alpha_s)$ processes of boson-gluon fusion (BGF) and QCD Compton. The ratio :

$$R_{(2+1)} = \frac{(2+1)\ jet\ X-section}{Total\ X-section} = c\alpha_s \tag{10}$$

where c is a function of y_{cut} and the event kinematics, shows that the $(2+1)$ jet rate is directly proportional to α_s. Therefore, by fixing y_{cut} and x, the ratio $R_{(2+1)}$ versus Q^2 yields $\alpha_s(Q^2)$. Figure 9a shows $R_{(2+1)}$ versus Q^2 from the H1 analysis using a y_{cut} of 0.02, but allowing both x and Q^2 to vary. The observed rate is consistent with an increase in the $(2+1)$ jet rate with Q^2 due to the increasing phase space available when the kinematics are not fixed. Figure 9b shows the ZEUS result, but with the

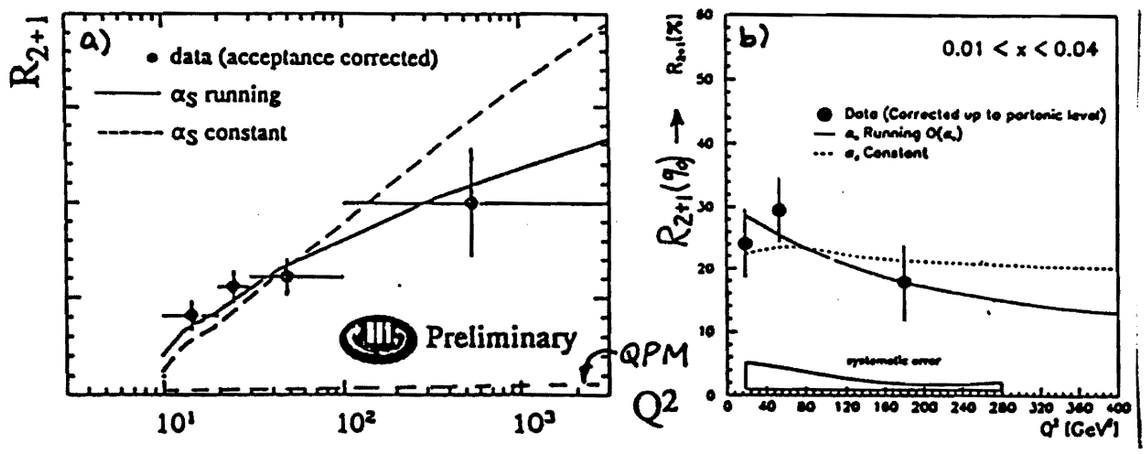

Figure 9: Preliminary $R_{(2+1)}$ versus Q^2 for $y_{cut} = 0.02$ from (a) H1, compared to the values from the ME+PS Monte Carlo generated with constant α_s and with running α_s, and (b) ZEUS, compared to the $\mathcal{O}(\alpha_s)$ calculation with running α_s and with constant α_s.

kinematics fixed by choosing a small x range ($0.01 < x < 0.04$). The observed rate shows the expected decrease in α_s as a function of Q^2 for fixed kinematics.

Evident in both the H1 and ZEUS multi-jet analyses is the ability to measure the Q^2 dependence of α_s in a single experiment. With an increase in data of a factor of ~ 10 expected in the current year and with the availability of higher order α_s calculations, both the value of α_s and its Q^2 dependence will be measured at HERA.

4.3. Charged Current DIS

At HERA, the large maximum Q^2 attainable ($Q^2 \gg M_W^2$) means that charged current events should be seen. Between the detectors H1 and ZEUS, for the luminosity achieved in the first years run, it was expected that ~ 1 charged current event should be seen by each detector. Both detectors have seen at least 1 charged current event; Figure 10a shows a candidate event of $Q^2 = 1815\ GeV^2$ in the H1 detector and Figure 10b shows a candidate event of $Q^2 = 14000\ GeV^2$ in the ZEUS detector[17].

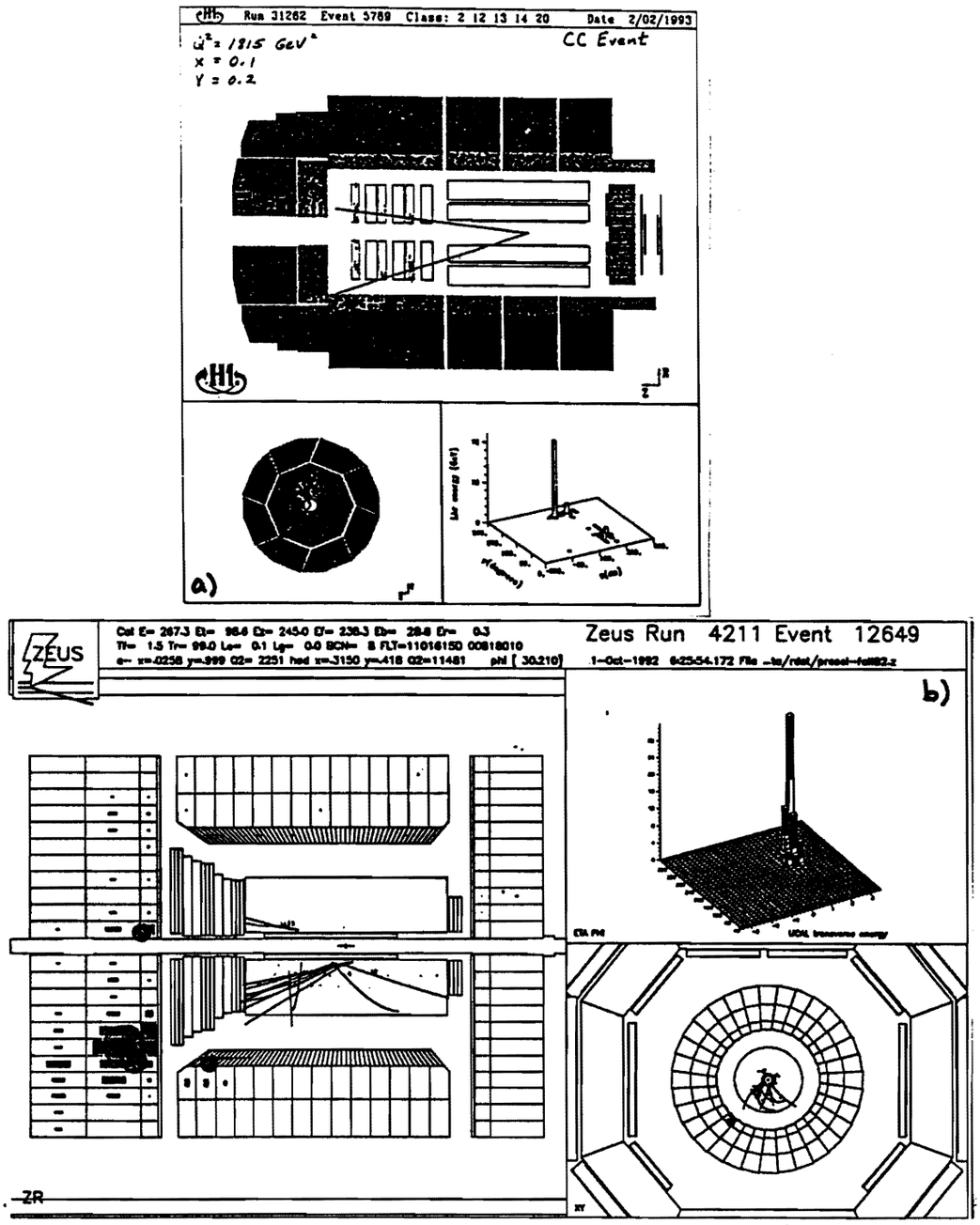

Figure 10: Charged current event in (a) the H1 detector ($Q^2 = 1815\ GeV^2, x = 0.1, y = 0.2$), and (b) the ZEUS detector ($Q^2 = 14000\ GeV^2, x = 0.44, y = 0.35$).

4.4. Events with Large Rapidity Gaps from ZEUS

It was noticed by the ZEUS collaboration that there is present in the data sample a subset of events in which no evidence of the fragmentation of the proton remnant is seen. In DIS events, most of the energy of the proton remnant is carried down the forward beampipe, but the tail of the remnant fragmentation distribution is seen as a large energy deposit in the cells of the FCAL around the beampipe. In subsequent comparisons with DIS Monte Carlos, a clear excess of events with very little energy around the forward beampipe (FCAL energy $< 1\ GeV$) is seen in the data. This excess also shows up as a small maximum pseudorapidity ($\eta_{max} < 1.5$) of the calorimeter condensates in an event when compared to the DIS Monte Carlo. Since the edge of the FCAL corresponds to $\eta \sim 4$, this means that there is a pseudorapidity gap of > 2 units present in these events, which is not described by the QCD based fragmentation models used in the Monte Carlo and is also not typical of DIS data (see Figure 8). Diffractive dissociation of the virtual photon involving pomeron exchange in DIS is expected to produce events with large rapidity gaps[18]. Furthermore, in the pomeron description of diffractive scattering, the rapidity distribution of the recoiling hadrons is expected to be flat. Figure 11 shows the the distribution of the maximum pseudorapidity (η_{max}) which is related to the pseudorapidity of the recoiling hadronic state. For $\eta_{max} < 1.5$, the excess of events in

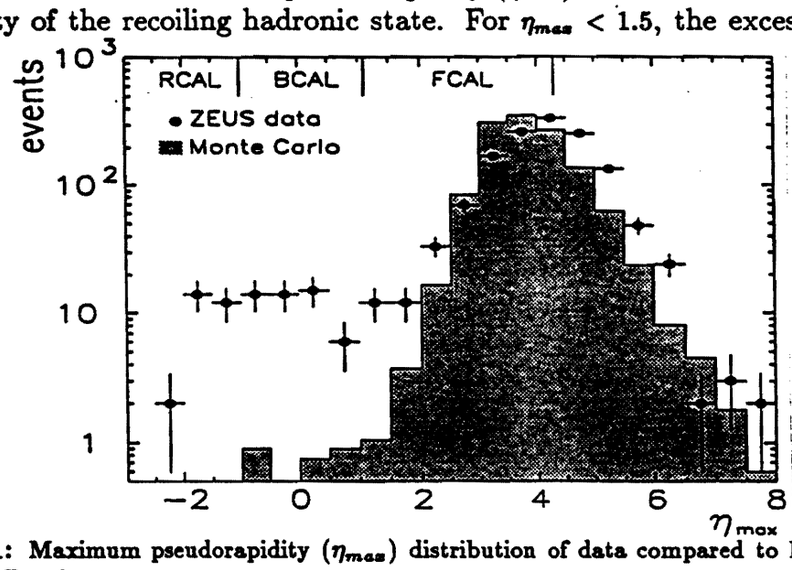

Figure 11: Maximum pseudorapidity (η_{max}) distribution of data compared to DIS Monte Carlo with no diffractive events.

the data compared to the non-diffractive Monte Carlo exhibits a flat distribution, consistent with the pomeron description of diffractive scattering. In Figure 12 the mass distribution of the recoiling hadronic system in the data sample given by :

$$M_x^2 = (\sum_{cal} E)^2 - (\sum_{cal} E_x)^2 - (\sum_{cal} E_y)^2 - (\sum_{cal} E_z)^2 \tag{11}$$

is shown as a function of the invariant mass W of the event for the whole DIS sample.

The distribution shows that there is a correlation between the invariant mass as

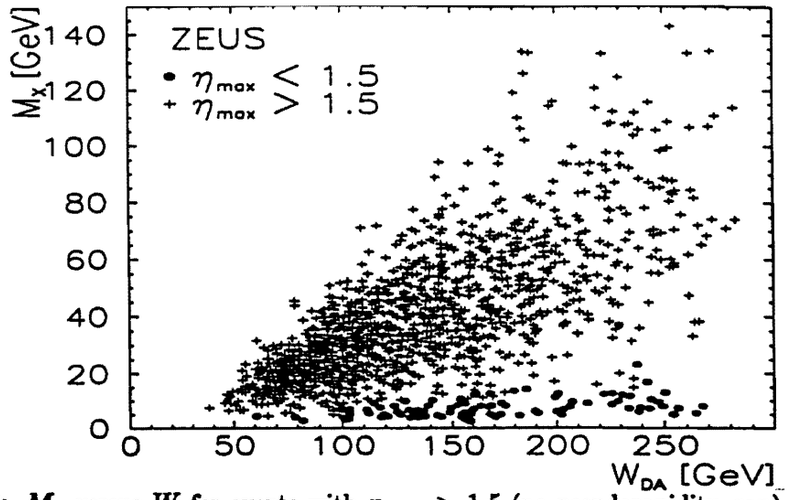

Figure 12: M_x versus W for events with $\eta_{max} > 1.5$ (no pseudorapidity gap) and $\eta_{max} < 1.5$ (pseudorapidity gap > 2).

seen in the calorimeter (M_x) and the invariant mass calculated from the kinematic variables (W) for the events with $\eta_{max} > 1.5$, while the events with $\eta_{max} < 1.5$ are characterized by small M_x which is nearly independent of W.

The presence of a pseudorapidity gap, the flatness of the η_{max} distribution, and the invariant mass distribution of the hadronic final state are all characteristics of diffractive scattering mediated by pomeron exchange between a virtual photon of high Q^2 and the proton.

5. Conclusions

The first year of data-taking at the HERA e-p collider has been successfully completed, with both detectors, H1 and ZEUS, reporting results on a wide variety of physics topics. Perhaps the most anticipated result was the low x behavior of the proton structure function, F_2. Both experiments have reported consistent results showing a large rise in F_2 at x values two orders of magnitude lower than previously measured. Studies of QCD effects in the hadronic energy flow have verified qualitative features of parton fragmentation and have rejected some specific Monte Carlo models consistently in both experiments. Multi-jet events have been seen in DIS and the ability to use them to measure basic QCD quantities has been demonstrated. Also, both experiments have seen charged current DIS events in numbers consistent with theoretical expectations. The ZEUS collaboration has reported the observation of events exhibiting large rapidity gaps, with a cross section consistent with theoretically predicted Pomeron exchange. In addition to the above results, both H1 and ZEUS have published papers on the DIS cross sections, the total photoproduction cross section, observation of resolved photoproduction, and mass limits from seaches for leptoquarks, leptogluons, and excited leptons[3,14,15,17,19].

Improvements and upgrades to both detectors and the anticipated large increase in delivered luminosity by HERA in the current year will yield additional physics results in the near future.

6. Acknowledgement

Work supported in part by the U. S. Department of Energy, Division of High Energy Physics, under contract W-31-109-ENG-38.

7. References

1. *HERA. A Proposal for a Large Electron - Proton Colliding Beam Facility at DESY*, (1981), and DESY preprint HERA 81-10, (1981).
2. F. W. Brasse, *The H1 Detector at HERA*, Invited talk, Proc. of the 26th Int. Conf. on High Energy Physics, (1992) and DESY preprint 92-140 (1992).
   H1 Collaboration, *Technical Proposal for the H1 Detector*, (1986).
3. ZEUS Collaboration: M. Derrick et. al., *Phys. Lett.* **B293** (1992) 465.
   ZEUS Collaboration, *The ZEUS Detector. Technical Proposal*, (1986).
4. M. Derrick et. al., *Nucl. Instrum. Methods* **A309** (1991) 77.
   A. Anderson et. al., *Nucl. Instrum. Methods* **A309** (1991) 101.
5. A. Bernstein et. al., *submitted to Nucl. Instrum. Methods.*
6. C. B. Brooks et. al., *Nucl. Instrum. Methods* **A283** (1989) 477.
   N. Harnew et. al., *Nucl. Instrum. Methods* **A279** (1989) 290.
7. S. Bentvelsen, J. Engelen, and P. Kooijman, *Proc. of the Workshop in Physics at HERA* **Vol 1**, edited by W. Buchmüller and G. Ingelman (Hamburg), (1991) 23.
8. P. Amaudruz, et. al., *Phys. Lett.* **B295** (1992) 159.
   A. C. Benvenuti et. al., *Phys. Lett.* **B237** (1990) 592.
   L. W. Whitlow et. al., *Phys. Lett.* **B250** (1990) 193.
9. CTEQ Collaboration: J. Botts et. al., *Phys. Lett.* **B304** (1993) 159.
   M. Glück, E. Reya, and A. Vogt, *Phys. Lett.* **B306** (1993) 391.
   A. D. Martin, R. G. Roberts, and W. J. Stirling, *Phys. Lett.* **B306** (1993) 145.
10. G. Ingelman, *Proc. of the Workshop in Physics at HERA* **Vol 3**, edited by W. Buchmüller and G. Ingelman (Hamburg), (1992) 1366.
11. M. Bengtsson et. al., *Phys. Lett.* **B301** (1988) 554.
    M. Bengtsson and T. Sjöstrand, *Z. Phys.* **C37** (1988) 465.
12. G. Gustafson, *Phys. Lett.* **B175** (1986) 453.
    G. Gustafson and U Petersson, *Nucl. Phys.* **B306** (1988) 746.
13. G. Marchesini and B. R. Webber, *Nucl. Phys.* **B310** (1988) 461.
14. H1 Collaboration: T. Ahmed et. al., *Phys. Lett.* **B298** (1993) 469.
15. ZEUS Collaboration: M. Derrick et. al., *Z. Phys.* **C59** (1993) 231.
16. JADE Collaboration: W. Bartel et. al., *Z. Phys.* **C33** (1986) 23.
    JADE Collaboration: S. Bethke et. al., *Phys. Lett.* **B213** (1988) 235.
17. ZEUS Collaboration: M. Derrick et. al., *Phys. Lett.* **B306** (1993) 173.

18. G. Ingelman and P. E. Schlein, *Phys. Lett.* **B152** (1985) 256.
A. Donnachie and P. V. Landshoff, *Phys. Lett.* **B191** (1987) 309.
K. H. Streng, *Proc. of the HERA Workshop* **Vol 1**, edited by R. D. Peccei (Hamburg), (1987) 365.
19. H1 Collaboration: T. Ahmed et. al., *Phys. Lett.* **B299** (1993) 385.
H1 Collaboration: T. Ahmed et. al., *Phys. Lett.* **B297** (1992) 205.
H1 Collaboration: T. Ahmed et. al., *Phys. Lett.* **B299** (1993) 374.
ZEUS Collaboration: M. Derrick et. al., *Phys. Lett.* **B297** (1992) 404.
ZEUS Collaboration: M. Derrick et. al., *Phys. Lett.* **B303** (1993) 183.
ZEUS Collaboration: M. Derrick et. al., *Phys. Lett.* **B306** (1993) 158.

NAME
I.D. No.
M.S.
RETURN TO FERMILAB LIBRARY